frontiers in Materials

ORIGINAL RESEARCH
published: 09 June 2021
doi: 10.3389/fmats.2021.630137

Archaeometrical Characterization of Romanian Late Bronze Age Ceramic Fragments

*Irina Fierascu[1], Anda Maria Baroi[1], Roxana Ioana Brazdis[1], Toma Fistos[1], Cristian Andi Nicolae[1], Valentin Raditoiu[1], Ioan Constantin Inel[2], Victor Sava[3] and Radu Claudiu Fierascu[1]**

[1]Emerging Nanotechnologies Group, National Research and Development Institute for Chemistry and Petrochemistry–ICECHIM Bucharest, Bucharest, Romania, [2]National Museum of the Union, Alba Iulia, Romania, [3]Arad Museum Complex, Arad, Romania

Knowledge of the past can provide information to protect the future and the potential of the technological development in the analytical sciences can be successfully applied for the study and conservation of cultural objects. In this context, in the present paper we propose an analytical methodology to characterize seven samples of ancient ceramic objects (dating to the Late Bronze Age). The samples were analyzed using optical microscopy, and all the samples presented a strong inhomogeneity on the surface, as suggested by the different colors of the ceramics. X-ray fluorescence (XRF) results reveal a relatively heterogenous composition of the samples, as well as strong differences between the different surfaces of each sample. By comparative analysis of the diffractograms recorded for both sides of the same samples were observed some differences, especially in terms of relative concentration of the component minerals, and, in lesser content, in terms of new phases present in the samples. Corroborated results obtained by XRF and X-ray diffraction (XRD) offered information regarding mineralogical composition of the samples: for some of them illite/muscovite and plagioclase phases are present in higher quantities or a lower quartz content. The presence of these components was confirmed by Fourier-transform infrared spectroscopy (FTIR) analysis. The thermal analysis completes the analytical investigation of the ceramic samples. The thermal behavior of the sample conducted to some explanation regarding the observed differences, due to the raw materials (that the major clay mineral in the samples is represented by illite) or to environmental factors during their burial in the soil.

Keywords: late bronze age ceramics, analytical characterization, thermal analysis, mineralogical composition, X-ray fluorescence spectroscopy, X-ray diffraction

OPEN ACCESS

Edited by:
Tadeusz Hryniewicz, Koszalin University of Technology, Poland

Reviewed by:
Ornella Cavalleri, University of Genoa, Italy
Sudagar J., VIT-AP University, India
Guosong Wu, Hohai University, China

****Correspondence:***
Radu Claudiu Fierascu
radu_claudiu_fierascu@yahoo.com

Specialty section:
This article was submitted to Environmental Materials, a section of the journal Frontiers in Materials

Received: *16 November 2020*
Accepted: *26 May 2021*
Published: *09 June 2021*

Citation:
Fierascu I, Baroi AM, Brazdis RI, Fistos T, Nicolae CA, Raditoiu V, Inel IC, Sava V and Fierascu RC (2021) Archaeometrical Characterization of Romanian Late Bronze Age Ceramic Fragments. Front. Mater. 8:630137. doi: 10.3389/fmats.2021.630137

INTRODUCTION

Ever since the inscriptions regarding human activity are known, ceramics were used as materials serving for cooking, storage, transport, construction, or pyrotechnical processing (Hein and Kilikoglou, 2018). Originally, these objects were made as practical tools for daily habits and later they were developed into works of art (Sun et al., 2020). The study of these objects enhance the horizons of knowledge of human traditions and regional history (Fierascu et al., 2020) and also allows the obtaining of a mineralogical characterization of raw materials (Drebushchak et al., 2018).

FIGURE 1 | Images of the analyzed ceramic fragments: **(A–G)**–samples 1–7.

The potential of the technological development in the analytical area can be successfully applied for the study and conservation of cultural objects (Papadopoulou et al., 2006a). Through an interdisciplinary approach, using analytical techniques and historians' and archaeologists' information, a complex characterization of ancient ceramics can be obtained, with the description of their mineralogical, chemical and thermal properties (Papadopoulou et al., 2006b). In this context, using a complex of analytical techniques such as thermal analysis, X-ray powder diffraction (XRD), petrography, and scanning electron microscopy (SEM), Drebushchak and coworkers discovered that calcite content of ceramic samples from late Bronze to early Iron Age (VIII-VI centuries BC) and early Iron Age (VII-IV centuries BC) represents a valuable parameter, useful for the identification of the clay sources (Drebushchak et al., 2005). The estimation of firing temperature of Persian haft rang tiles was performed using the phase transformations in calcareous clay bodies during firing and X-ray diffraction patterns (Holakooei et al., 2014). These techniques are not suitable only for chemical and mineralogical characterization; they can also be used in order to identify the causes of different degrees of degradation (Kloužková et al., 2016) and to identify diagnosis methods required for restoring (Duran et al., 2010). Also, analytical results can lead to a superior understanding of the local ceramic production and the exchange pattern between the adjacent regions (Gutsuz et al., 2017).

The characterization of ancient ceramics can be definitely completed by differential thermal analysis (DTA) and thermogravimetric (TG) measurements, the temperature at which ancient ceramics were fired varying in a wide range (600–1,300°C), depending on the type of clay used and the kiln available (Ponta et al., 2016); meanwhile, other type of analysis offers mineralogical and geochemical information (Ionescu et al., 2014).

In this context, the aim of the present paper is to obtain a complex characterization of seven samples of ancient ceramic objects (from Late Bronze Age) through thermal analysis, X-ray diffraction, X-ray fluorescence, Fourier-transform infrared spectroscopy, and optical microscopy, in order to provide information regarding raw materials used in the past and to identify the effects of time and burial conditions on their composition.

MATERIALS AND METHODS

Investigated Materials and Archaeological Context

Investigated Materials

The ceramic objects were collected from two sites (Pecica–Site 14 and Sântana–Cetatea Veche—*Old Fortress*; position of the two archaeological sites is presented in **Supplementary Figure S1**) being dated to the Late Bronze Age (LBA) (Gogaltan et al., 2010; Ignat and Sava, 2019). The ceramic fragments were provided by courtesy of the Arad Museum Complex of (Romania) for analytical study. The samples are presented in **Figure 1**, detailed in **Table 1**, while the archeological context is presented in **Supplementary Figure S2**.

Historical Context

Pecica–site 14. During 2011, a cemetery near Pecica, Arad County, was discovered and investigated. In the area of 7762 m^2, 38 graves were identified, of which 24 were burial and 14 cremation graves. From the chronological point of view, 10 can certainly be attributed to the Late Bronze Age I (LBA I) stage (eight buried and two cremation), another six cremation and one burial grave belonging to LBA II, while 15 burial graves and cremation cannot be accurately assigned to a specific stage, due to the lack of typical inventory. The funeral inventories consist of bronze pieces (weapons—daggers and axes and jewelry—bracelets, needles, apices), amber pieces and ceramics (the typical inventory consists of a pot and one or

TABLE 1 | Characteristics of the analyzed ceramic fragments.

Sample	Archaeological site	Archaeological context (Cx.)	Details	Site absolute dating
1	Pecica—site 14	Cx. 30 (cremation grave)	Part of the funeral urn	Approx. 1,600/ 1,550–1300 BC
2	Pecica—site 14	Cx. 78 (cremation grave)	Part of the funeral urn	Approx. 1,600/ 1,550–1300 BC
3	Pecica—site 14	Cx. 92 (cremation grave)	Part of a vessel buried in the grave	Approx. 1,600/ 1,550–1300 BC
4	Sântana—old fortress	S1, carriage 64	Part of a "mobile fireplace"	Approx. 1,450–1,300/ 1250 BC
5	Sântana—old fortress	S1 Cx. 40 (cremation grave)	Part of the funeral urn	Approx. 1,450–1,300/ 1250 BC
6	Sântana—old fortress	S1 Cx. 38 carriage 74B (defense channel of fortification III)	Part of an entire vessel discovered in the fort's defense channel	Approx. 1,450–1,300/ 1250 BC
7	Sântana—old fortress	S1 Cx. 2 (pit)	Ceramic fragment found in the filling of the pit	Approx. 1,450–1,300/ 1250 BC

two bowls), the graves of children and adolescents being the richest. Chronologically, it appears that the cemetery is functional from LBA I, but it is still used throughout LBA II (Sava et al., 2019).

Sântana–Cetatea Veche. The Sântana fortification is located in the plain area of the Lower Mures Basin, more precisely in the west of Romania, about 25 km north of the city of Arad. New archaeological investigations on the "Cetatea Veche" site have been undertaken since 2008. The accidental discoveries and the archaeological excavations carried out so far show us the image of a dynamic fortification that encloses an area of over 130 ha. The four fortification systems composed of earth waves, defense ditches and large palisades began to be built during the 15th century BC and continue to be used until the end of the 13th century BC. The multiple researches carried out on various occasions offer consistent indications regarding the intensity of the habitation; this is reflected by the numerous pieces of gold, bronze, copper, ceramic fragments, and burnt remains of large structures (Gogaltan et al., 2019a).

Further specific details regarding the particular archaeological contexts are provided in the **Supplementary Material**.

Analytical Methods

The samples were analyzed using optical microscopy, thermal analysis, X-ray fluorescence, X-ray Diffraction and Fourier transform infrared spectroscopy, using a previously proposed methodology (Fierascu et al., 2020). Given the specific shape of the ceramic pieces and the burial conditions, all samples were analyzed on both sides, results being presented as Sample Xa for the concave surface (interior of the vessels), respectively Sample Xb for the convex surface (exterior of the vessels).

Optical microscopy was used in order to observe any surface features present on the surface, as well as to visualize the possible inclusions in the ceramic pieces (El Amraoui et al., 2017); the microscopical evaluation was performed using an OPTIKA B-150DBR optical microscope.

For the assessment of the ceramic elemental composition, a completely non-destructive and non-invasive method was selected, respectively X-ray fluorescence spectrometry, using a portable XRF spectrometer Olympus VANTA C (40 kV X-ray tube with rhodium anode, Silicon Drift Detector, in Geo-Chem configuration, acquisition time 60 s for each beam, internal calibration). The equipment uses two different energy beams for the quantification of the elements: beam 2 (10 kV) for light elements (Mg, Al, Si, P, S, K, Ca, Ti, Mn) and beam 1 (40 kV) for the rest of detectable elements. The portable variant of the technique was selected, as the bench-top configuration (presented in our previous studies) would request some degree of sampling, due to the limitation of the equipment (Fierascu et al., 2020). The phase composition of the samples was evaluated using X-ray diffraction analyses, performed using a Rigaku SmartLab equipment, operated at 45 kV and 200 mA, CuKα radiation (1.54059 Å), parallel beam configuration (2θ/θ scan mode). The individual components were identified using the Rigaku Data Analysis Software PDXL 2, database provided by ICDD. As was the case for the XRF analysis, sampling was not necessary for the XRD determinations, neither (a representative image obtained during XRD analysis is presented in **Supplementary Figure S3**.

In order to further elucidate the characteristics of the ceramic samples, FTIR analyses were performed using a Jasco FTIR 6,300 spectrometer equipped with a Specac ATR Golden Gate (KRS5 lens), in the 400–4,000 cm^{-1} range (32 accumulations at a resolution of 4 cm^{-1}, scanning speed 2 mm/s). Finally, thermal analyses were performed on a Q5000IR instrument (TA Instruments), using 100 μL platinum sample pans, at a heating rate of 10 °C/min, from room temperature to 1,000 °C, using synthetic air (99.999%) as purge gas (50 ml/min).

For FTIR and thermal analyses, a few milligrams (typically around 10 mg) of ceramic material were liberated from each side of the samples using a scalpel blade, without visibly damaging the artefacts.

RESULTS AND DISCUSSIONS

The Late Bronze Age is one of the most dynamic periods in the Carpathian Basin prehistory. If during the Middle Bronze Age

(approx. 2,000–1,550 BC) stable systems were developed, characterized in the plain area by tell type settlements, successive habitations in the same space for several generations, LBA shows a different evolution. The Lower Mure Basin, a region where the *Pecica-Site 14* and *Sântana-Cetatea Veche* sites are being developed, is an integral part of the Carpathian Basin, but at the same time has special characteristics. The gradual abandonment of the tells, occurring after about 1,650/1,600 BC (Gogaltan et al., 2015), coincides with the appearance of a small number of new settlements and cemeteries attributed to LBA I (approx. 1,550–1,450 BC). In this chronological stage, LBA 1 (approx. 1,600/1,500–1,500/1,400 BC), it can be noticed a repositioning of the network of settlements at the foot of the Apuseni Mountains, probably due to the flow of raw materials that connected the mountainous area to the lowland areas. It seems that in some settlements, such as *agu Site* "*A1_1*," both notable metallurgical and agricultural activities were carried out (Sava et al., 2011; Sava et al., 2012). Now the bronze pieces are widely spread, but the funerary practices encountered in the cemetery from *Pecica-Site 14* indicates major accumulations of bronze in a small number of graves (Ignat and Sava, 2019). After more than 100 years since the abandonment of the tells, between 1,500–1,400 BC, only in the Lower Mures Basin is started the building of complex fortification systems, surrounding hundreds, even thousands of hectares that are developed throughout the LBA II period (approx. 1,450–1,250 BC). Among the most representative mega-forts are *Cornesti-Iarcuri*, whose fortification systems surround a huge area of 1,765 ha (Krause et al., 2016) and *Sântana-Cetatea Veche*, which although it covers a fortified area of only 130 ha highlights through the richness of the findings (Gogaltan et al., 2010; Gogaltan et al., 2019a; Gogaltan et al., 2019b). Around these mega-forts there is a dense network of unfortified settlements, some inhabited since LBA I (Sava et al., 2019). Medium and long-distance trade, the intensity of metallurgical and agricultural production generated unprecedented accumulations of wealth during LBA II, reflected in three hoards of gold ornaments and numerous bronze deposits. During the 13th century B.C., it can be observed in the Lower Mures Basin a series of violent destructions of the major fortifications (Gogaltan et al., 2019a; Lehmphul et al., 2019; Sava, 2019; Molloy et al., 2020). It should be noted that the number of discoveries associated with LBA III (approx. 1,250–900 BC) is significantly decreased. With the destruction of the fortification from *Sântana* and gradually of the other mega-forts, but also the abandonment of unfortified settlements, processes that took place mainly between 1,300 and 1,200 BC, the Lower Mures Basin enters a collapse reflected by the drastic decrease in the number of settlements. bronze and exotic goods. At the same time, new centers of power appear in Transylvania and northeastern Hungary (Bălan et al., 2013).

Recently, a series of analyzes on the stylistic evolution of ceramics in the Lower Mures Basin were published, starting from consistent series of radiocarbon data, which highlight the main trends of ceramic shapes and decorations (Sava, 2019; Sava, 2020). However, the stylistic characterization of those artifacts should be doubled by thorough archaeometrical studies.

As a first step of the archaeometrical protocol, the samples were analyzed using optical microscopy (representative images presented in **Figure 2**, other images provided in **Supplementary Material Figure S4**).

As can be observed from the optical microscopy images presented, all the samples presented a strong inhomogeneity on the surface, as suggested by the different colors of the ceramics. Most probable minerals, as revealed by the optical microscopy are quartz, calcite, mica, and grog (added materials) (El-Gohary et al., 2019). More than, that, all samples (especially visible in the case of sample 3a) present crystals on surface, most probably due to salt migration and crystallization (efflorescence phenomena) (Paterakis and Steiger, 2015).

The results of the XRF analysis are presented in **Table 2** (examples of XRF spectra provided in **Supplementary Figure S5**). Given that the portable XRF instruments have a spot size smaller than 1 cm (in diameter) (Crocombe, 2018), multiple determinations are often required to provide a statistically significant determination of the samples' composition (Fierascu et al., 2017).

The results reveal a relatively heterogenous composition of the samples (considering the high SD values), as well as strong differences between the different surfaces of each sample. The highest differences are recorded for sample seven. This was expected, considering the major visual differences recorded for this particular sample (see **Supplementary Figure S6**). However, these differences should be confirmed by phase identification (XRD analyses–diffractograms presented in **Figure 3**, assignment of the diffraction peaks presented in **Supplementary Table S1**).

The X-ray diffraction analyses revealed a composition dominated by quartz (PDF card no. 01-070-7344), plagioclase (PDF card no. 01-083-1371), kaolinite–PDF card no. 00-001-0527, and illite/muscovite–PDF card no. 00-002-0056/01-072-0496). Traces of calcite (PDF card no. 01-083-0577) and feldspar (PDF card no. 01-075-9267) were also identified on some of the samples. A common trace mineral in all the samples was hematite (PDF card no. 01-072-6226).

By comparative analysis of the diffractograms recorded for both sides of the same samples, it can be observed some differences, especially in terms of relative concentration of the component minerals, and, in lesser content, in terms of new phases present in the samples. Thus, for Sample 1, the major difference is represented by the different intensity of the peak appearing at approx. 29.4° (sample 1a, high intensity), which, corroborated with the results presented in **Table 2**, is most probably due to the presence of calcite in Sample 1a, respectively its absence in Sample 1b. This is also the case of sample 3, for which the concave side (3a) presents well defined peaks associated with the calcite phase, while sample 3b presents stronger peaks, associated with mica (see **Supplementary Table S1**), and sample 5, in which the calcite phase is also present on the concave side (5a). These findings are also supported by the strong differences between the calcium content (presented in **Table 2**). Sample 2 presents a relatively uniform composition (in qualitative terms), the intensity differences recorded, correlated with the XRF results suggesting differences in terms of calcite content

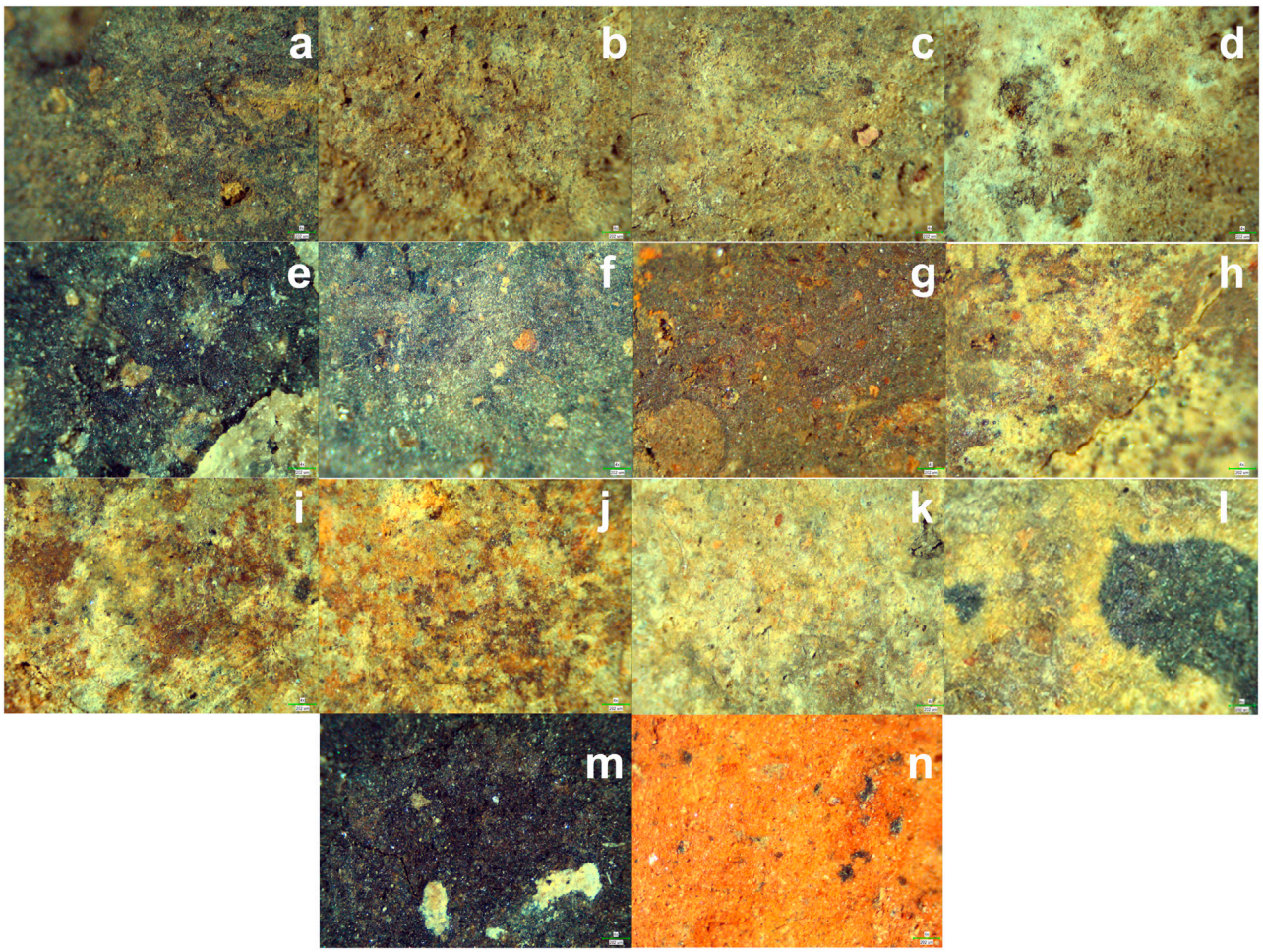

FIGURE 2 | Optical microscopy images of the analyzed samples: **(A,B)**–sample 1a/b; **(C,D)**–sample 2a/b; **(E,F)**–sample 3a/b; **(G,H)**–sample 4a/b, 4x magnification; **(I,J)**–sample 5a/b; **(K,L)**–sample 6a/b; **(M,N)**–sample 7a/b; all images are recorded at 4x magnification, scale provided on individual images.

(phase present on both sides). A similar observation can be made for sample 4, in which the illite/muscovite and plagioclase phases are present in considerably higher amount on sample 4b, compared with 4a (as suggested by the peaks appearing at approx. 13.8°, 27.8°, 55.8°, respectively 66.6°; for the last peak, the contribution of kaolinite is also considerable). Sample 6, on the other hand, presents a similar composition on both sides, both in terms of elemental and mineralogical composition, the only differences being recorded in terms of illite/muscovite and plagioclase content (higher in sample 6b, associated with the variation of the peaks appearing at approx. 8.8°, 22.9°, respectively 41.2°). The strongest visual differences, recorded for sample 7, can hardly be explained considering the XRD analysis. Thus, a minor calcite content is present on sample 7a, while the illite/muscovite and plagioclase phases are present in higher quantities in sample 7b (as suggested by the XRF results). Also, the peaks corresponding to quartz (see **Supplementary Table S1**) present lower intensity for sample 7a, compared with sample 7b; this aspect, corroborated with the results presented in **Table 2**, suggests a lower quartz content, while the very high content in light elements recorded for sample 7a remains to be explained by other analytical techniques. The hematite content appears to remain relatively constant in all the analyzed samples, as the iron content recorded by XRF would suggest.

The rest of the elements identified by XRF and not assigned to any phase by XRD are most probably impurities in the clay materials used as raw materials. Also, the Rb, Zr, and Sr content (relatively constant for all the analyzed samples) could represent an indicator regarding the origin of the raw materials, as previously presented by our group (Fierascu et al., 2020).

Other important aspects that can be revealed from the XRF results are represented by the chemical index of alteration (CIA), index of compositional variance (ICV), respectively the Rb-Fe-Sr, Al_2O_3-Fe_2O_3-SiO_2, and Al_2O_3-CaO-Fe_2O_3 scattergrams, which can be used to place the analyzed samples in the context of other LBA ceramic artifacts (details regarding the methodology for the calculation of CIA and ICV are provided in other studies, as well as in the **Supplementary Material**). The scattergrams are presented in **Figure 4** and **Supplementary Figure S7**.

TABLE 2 | XRF composition of the samples. Results are presented in mg/kg unless other measurement units are provided and represent the average of five determinations on randomly selected points ± SD.

Element/ Sample	Si (%)	Al (%)	Fe (%)	Mg[a] (%)	K (%)	Ca (%)	Ti	P	S	V	Cr	Mn	Ni	Cu	Zn	Sr	Zr	Rb	L.E. (%)
1a	15 ± 3	6 ± 1	4.2 ± 0.5	1 ± 2	1.3 ± 0.2	4 ± 1	4,640 ± 640	950 ± 350	95 ± 55	113 ± 35	55 ± 9	1860 ± 100	70 ± 15	66 ± 12	112 ± 11	188 ± 7	177 ± 7	108 ± 5	63 ± 5
1b	11 ± 2	2.9 ± 0.7	4.9 ± 0.7	n.d	1.1 ± 0.3	0.9 ± 0.2	5,380 ± 340	450 ± 80	52 ± 17	128 ± 36	91 ± 48	969 ± 71	100 ± 18	42 ± 12	113 ± 12	153 ± 3	168 ± 6	129 ± 5	78 ± 4
2a	13 ± 3	5 ± 1	3.6 ± 0.6	n.d	1.4 ± 0.2	6 ± 3	4,173 ± 648	1,676 ± 984	75 ± 30	90 ± 37	57 ± 5	1,278 ± 31	87 ± 4	48 ± 12	107 ± 11	156 ± 6	184 ± 15	110 ± 7	70 ± 4
2b	8 ± 2	3.1 ± 0.6	2.3 ± 0.7	n.d	0.7 ± 0.1	17 ± 4	2,983 ± 1,231	1,540 ± 99	n.d	63 ± 15	65 ± 33	1,139 ± 92	40 ± 19	32 ± 3	87 ± 24	161 ± 15	154 ± 26	96 ± 27	68.8 ± 0.7
3a	4 ± 2	1.5 ± 0.6	2.8 ± 0.6	n.d	0.5 ± 0.3	15 ± 5	3,153 ± 839	1,540 ± 282	490 ± 63	69 ± 9	78 ± 51	231 ± 51	36 ± 8	48 ± 12	74 ± 15	170 ± 9	137 ± 9	107 ± 6	77 ± 6
3b	15 ± 4	5 ± 2	5.7 ± 0.4	n.d	1.5 ± 0.3	1.3 ± 0.1	4,600 ± 330	2021 ± 16	587 ± 39	105 ± 34	113 ± 20	926 ± 466	54 ± 9	63 ± 13	113 ± 13	156 ± 21	145 ± 6	130 ± 17	71 ± 6
4a	23 ± 4	9.5 ± 0.8	5.4 ± 0.7	1 ± 2	1.8 ± 0.4	0.60 ± 0.02	5,160 ± 300	250 ± 37	74 ± 19	34 ± 28	104 ± 39	1,017 ± 62	53 ± 12	89 ± 11	95 ± 9	106 ± 4	157 ± 5	113 ± 4	54 ± 3
4b	23 ± 3	9.4 ± 0.8	5.4 ± 0.5	n.d	1.8 ± 0.3	0.6 ± 0.2	6,100 ± 280	324 ± 49	59 ± 12	88 ± 27	150 ± 38	1,217 ± 60	127 ± 14	27 ± 8	113 ± 8	141 ± 4	197 ± 5	123 ± 4	59 ± 2
5a	18 ± 1	9.4 ± 0.4	4.4 ± 0.5	n.d	1.3 ± 0.3	2.2 ± 0.3	3,990 ± 270	600 ± 280	68 ± 18	158 ± 32	162 ± 45	5,230 ± 140	146 ± 16	107 ± 12	119 ± 10	186 ± 5	281 ± 6	102 ± 4	64 ± 2
5b	18 ± 1	8.4 ± 0.8	4.9 ± 0.6	n.d	1.3 ± 0.2	0.73 ± 0.02	3,770 ± 260	180 ± 42	46 ± 13	117 ± 29	94 ± 41	4,900 ± 130	203 ± 19	49 ± 10	149 ± 11	154 ± 5	292 ± 6	98 ± 4	66 ± 3
6a	25 ± 2	11 ± 1	5.8 ± 0.5	n.d	1.7 ± 0.2	0.6 ± 0.1	5,010 ± 210	650 ± 170	129 ± 99	68 ± 21	179 ± 31	291 ± 31	68 ± 10	168 ± 10	157 ± 8	116 ± 3	118 ± 3	124 ± 3	55 ± 3
6b	22 ± 2	10 ± 1	6.1 ± 0.5	n.d	1.5 ± 0.3	0.5 ± 0.1	4,010 ± 210	170 ± 45	540 ± 120	14 ± 23	70 ± 31	242 ± 31	51 ± 10	103 ± 9	139 ± 8	108 ± 3	115 ± 3	107 ± 3	59 ± 3
7a	17 ± 1	3.6 ± 0.4	3.5 ± 0.5	n.d	1.6 ± 0.3	1.2 ± 0.3	5,050 ± 320	247 ± 77	62 ± 12	15 ± 35	52 ± 33	520 ± 52	35 ± 13	101 ± 12	140 ± 11	156 ± 5	255 ± 6	127 ± 5	73 ± 4
7b	28 ± 4	7.7 ± 0.9	4.4 ± 0.7	0.6 ± 1.2	2.1 ± 0.4	0.6 ± 0.2	5,720 ± 300	910 ± 260	57 ± 18	37 ± 27	143 ± 39	890 ± 56	65 ± 12	72 ± 10	139 ± 9	124 ± 4	288 ± 7	110 ± 4	54 ± 4

[a]*L.E.–light elements; n. d.–not detected; in the case of Mg, the SD is higher than the average value due to the fact that the element was not quantified in all the five determinations.*

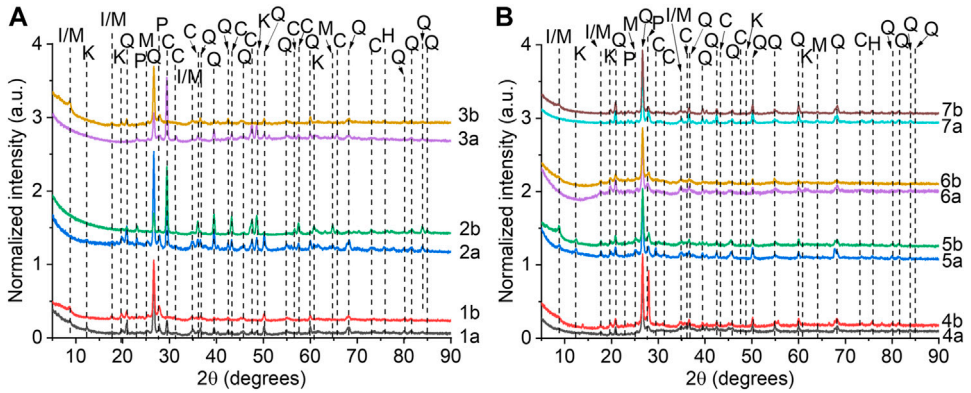

FIGURE 3 | X-ray diffractograms of the analyzed ceramic samples, showing most probable identification of the major peaks: **(A)** samples 1–3; **(B)** samples 4–7. I/M–illite/muscovite, K–kaolinite, P–plagioclase, C–calcite, Q–quartz, H–hematite.

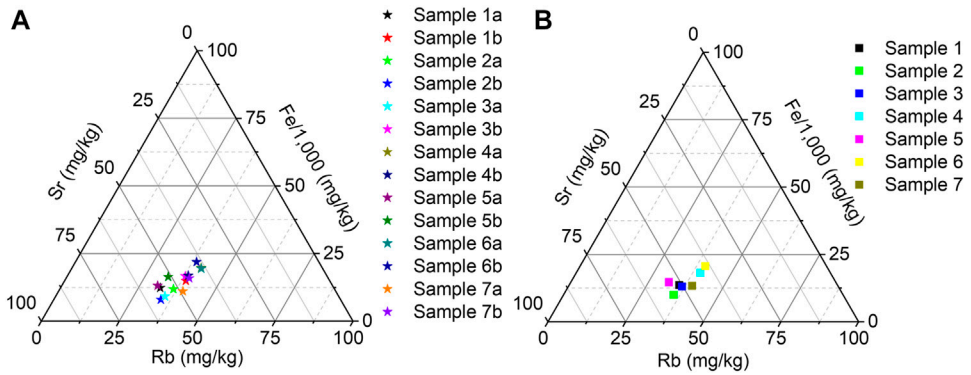

FIGURE 4 | Rb-Fe-Sr scattergram of the analyzed samples (differentiating between the concave and the convex side) **(A)** and of the averaged values per samples (average values of all the determinations performed on the concave and convex side) **(B)**.

Data in **Figure 4B** supports the proposal of a common origin of samples 1–3 (group 1), excavated from the same archaeological site. Interestingly, sample five and seven also presents similar characteristics with the group 1 samples (noteworthy is the fact that sample 5 was excavated from a very close area to samples four and six). Samples four and six also seem to share a common origin.

By plotting the averaged values per sample of the major elements Al_2O_3-Fe_2O_3-SiO_2 and Al_2O_3-CaO-Fe_2O_3 (presented in **Supplementary Figure S7**), the samples can also be defined. The shift recorded for sample 7 from the rest of the samples (presented in **Supplementary Figure S7a**) can be explained by the high differences recorded in terms of Si content between the two analyzed sides. The other samples have a similar composition on both sides (aspect also observed for other Romanian LBA ceramics previously analyzed (Fierascu et al., 2020). **Supplementary Figure S7b** allows the characterization of sample 2 as a Ca-rich ceramic, and aluminium-poor ceramic. The rest of the samples are also similar in the ternary composition to the ceramic samples previously presented by our group (Fierascu et al., 2020). Also, sample 2 resembles the composition of the LBA ceramics of Anatolian origin (Semiz et al., 2018).

TABLE 3 | Average values of CIA and ICV indices per sample.

Sample	CIA	ICV
1	64 ± 5	1.8 ± 0.3
2	33 ± 19	3 ± 2
3	42 ± 42	5 ± 5
4	85.48 ± 0.11	0.71 ± 0.06
5	83 ± 5	0.687 ± 0.001
6	88.4 ± 0.8	0.59 ± 0.03
7	73 ± 11	1.1 ± 0.4

The two proposed indices (CIA/ICV) are currently used by geologist to estimate the alteration/degradation of rocks (Nesbitt and Young, 1982; Cox et al., 1995). Lately, they were also applied for the characterization of archaeological ceramic samples (Diskin and Ashley, 2016; Hoeck et al., 2009). The average CIA levels (presented in **Table 3**) reveal the extent of the chemical

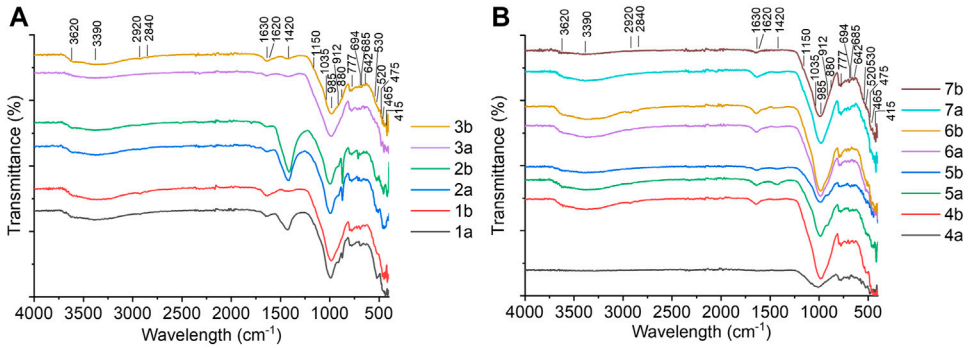

FIGURE 5 | FTIR spectra of the analyzed ceramic samples: **(A)** samples 1–3; **(B)** samples 4–7.

degradation of the ceramic samples: two of the samples (2 and 3) could be categorized as exhibiting "little degradation effect" (CIA<50), while the rest present moderate degradation effect (Diskin and Ashley, 2016). However, the two samples in question present fundamental differences when evaluating the two sides of the ceramic: if sample 2 presents values <50 of the CIA for both sides, sample 3 presents very low CIA value for the *a* side (<20) and a high value for the *b* side (>70). This could be explained by a selective surface degradation of the exterior side of the vessel. Significant differences between the CIA values recorded for the two sides were also observed for samples 1, 5, and 7, without affecting their general characteristic of "moderate degradation"; these results indicate that the raw materials used for ceramic manufacturing was subjected to moderate weathering/alteration at source, without undergoing multiple weathering and lithification cycles (supporting the hypothesis that the raw materials consisted of sediments derived directly from an igneous source).

The ICV values can range from 0.01 (clays) to 1,000 (non-clay silicates) (Cox et al., 1995; Hoeck et al., 2009). The results obtained for our samples suggest the contribution of added minerals into the clay. The results of all the samples fit the samples into a system characterized by the addition of muscovite/plagioclase minerals. The samples recording higher ICV values (2 and 3) could benefit from the contribution of a higher plagioclase/K-spar content (samples 2b and 3a) or from the calcite present in the samples (see also **Table 2**–calcium content), as other authors also noticed (Rizzo et al., 2016).

As a further step of the study, the FTIR spectra of the samples were recorded (presented in **Figure 5**).

The recorded FTIR spectra have similar characteristics, that will be discussed considering the most probable components that can be identified (considering the XRD results). Thus, the bands around 3,390 cm^{-1} and 1,630 cm^{-1} are related to moisture present in the ceramic samples (O-H stretching, respectively H-O-H bending) (Palanivel and Rajesh Kumar, 2011; Costa et al., 2017; Fierascu et al., 2020); the quartz, as a component found in all samples, can be defined by the bands appearing around 1,620 cm^{-1}, 777 cm^{-1}, 694 cm^{-1} and 520 cm^{-1} (Russell et al., 1994; De Benedetto et al., 2002; Ramasamy et al., 2009; Costa et al., 2017). The bands around 530 and 465 cm^{-1}, also present in all samples, correspond to the υ Fe-O stretching of the hematite form of iron oxide (Legodi and Dewaal, 2007), also observed by the XRD analysis. The peaks appearing around 2,840 and 2,920 in some samples (1b, 3a, 3b, 4b, 6b, 7a) could be assigned to the υ C-H stretching, suggesting the presence of organic material traces in the fragments (which could be correlated with the higher content in light elements determined by XRF). The very intense band appearing in all samples around 985 cm^{-1} can be assigned to muscovite with three Si atoms (Jordá et al., 2015); the same attribution can be made to the bands at 685, 475, and 415 cm^{-1} (bending of Si-O-Al group, bending of Si-O-Si group, and Al-OH vibrational modes, respectively) (Abukhadra and Mostafa, 2019). The presence of calcite in some of the samples (1a, 2a, 2b, 3a, 5a, 7a) is supported by the bands around 1,420 cm^{-1}, respectively 880 cm^{-1} (Ramasamy et al., 2009). The presence of the kaolinite mineral is suggested by the appearance of a peak around 1,030–1,040 cm^{-1}, as well as by the one at 912 cm^{-1} (Ricci et al., 2016). The weak FTIR bands suggest low amounts of kaolinite present in the samples. The presence of feldspar (identified by XRD in sample 1b) is suggested by the bands appearing at 1,150, 989 (overlapping with the muscovite band) and 642 cm^{-1} (Wang et al., 2018). The appearance of a band around 3,620 cm^{-1} can be assigned to the O–H str. from the clay minerals–kaolinite/illite (Ricci et al., 2016). Presence of plagioclase in the samples can hardly be confirmed by the FTIR analysis, as its specific bands (980–1,100 cm^{-1}, 740 cm^{-1}, 580 cm^{-1}, and 540 cm^{-1}) are overlapping the other components (Papakosta et al., 2020).

The thermal analysis completes the analytical investigation of the ceramic samples (TG/DTG curves presented in **Supplementary Figure S8**, data presented in **Table 4**). For understanding the nature of the materials, thermal analysis was performed on concave and convex sides of the samples, as well as on material collected from the interior of the samples (encoded as samples *Xc*). For sample 2, presenting white deposits on the convex surface (b) (visible in **Figure 1B**), were collected two samples (one avoiding the deposits–encoded sample 2b'–**Supplementary Figure S8e** and one with deposits–encoded sample 2b"–**Supplementary Figure S8f**); for sample 7, presenting two different colors (black on surface a and red on surface b), the interior material was collected from two

TABLE 4 | Main parameters of the processes as evidenced in TG and DTG curves.

Sample	RT-T_1	T_1	T_1-T_2		T_2	T_2-T_3		T_3	T_3-T_4		T_4	Up to 1,000 °C	Residue
	Wt loss (%)	°C	Wt loss (%)	T_{max} (°C)	°C	Wt loss (%)	T_{max} (°C)	°C	Wt loss (%)	T_{max} (°C)	°C	Wt loss (%)	At 1,000 °C (%)
1a	6.27	200	4.93	381.5	565	0.42	-	750	-	-	-	0.16	88.21
1b	5.71	200	6.40	390.1	565	3.24	653.5	750	-	-	-	-0.70	85.34
1c	4.57	200	2.90	367.7	565	0.28	-	750	-	-	-	0.22	92.04
2a	5.29	200	5.68	370.7	525	3.00	642.2	800	-	-	-	0.09	85.93
2b′	1.37	200	1.53	325.0	525	0.67	617.3	800	-	-	-	0.04	96.39
2b"	2.26	200	3.13	345.3	525	29.60	736.1	800	-	-	-	0.12	64.88
2c	1.94	200	1.23	331.4	525	0.83	645.2	800	-	-	-	0.28	95.72
3a	3.79	225	5.97	394.1	565	2.03	658.4	750	-	-	-	0.21	88.01
3b	5.27	225	5.97	394.1	565	0.96	678.7	750	-	-	-	0.24	87.00
3c	6.17	225	3.61	416.1	565	0.55	669.7	750	-	-	-	0.21	89.47
4a	6.38	220	3.07	372.1	800	-	-	-	-	-	-	0.14	90.41
4b	5.29	220	4.86	375.2	800	-	-	-	-	-	-	0.14	89.70
4c	9.16	220	4.80	356.3	800	-	-	-	-	-	-	0.20	85.83
5a	5.25	200	1.07	273.7	300	4.20	422.7	605	0.49	639.9	715	0.80	88.23
5b	5.72	200	1.08	271.0	300	4.50	422.2	605	1.21	647.2	715	0.80	86.64
5c	4.56	200	0.72	-	300	1.90	409.2	605	0.20	672.9	715	0.30	92.29
6a	6.19	210	0.89	256.6	290	4.12	448.5	680	1.25	769.2	1,000	-	87.55
6b	6.64	210	1.05	260.9	290	4.02	448.5	680	1.15	758.2	1,000	-	87.14
6c	0.85	210	7.12	262.2	290	4.03	408.8	680	1.28	743.1	1,000	-	86.73
7a	4.05	240	2.66	433.0	580	0.84	628.9	715	-	-	-	1.26	91.17
7b	3.28	240	1.86	414.5	580	0.83	640.6	715	-	-	-	0.71	93.32
7c'	4.36	240	2.69	421.4	580	0.40	-	715	-	-	-	0.70	91.85
7c"	3.43	240	1.51	418.1	580	0.39	-	715	-	-	-	0.77	93.89

Where: T_{max} (°C) = $T(d\alpha/dt)_{max}$.

sites, one closer to the black color–sample 7c' (**Supplementary Figure S8v**) and one closer to the red color, sample 7c" (**Supplementary Figure S8w**).

Most of the analyzed samples present a similar mass loss under 200 °C (approx. 2–6%) and similar endothermic effects, attributable to a dehydration process (respectively the loss of moisture water) (Palanivel and Rajesh Kumar, 2011; Shoval and Paz, 2013). Two samples have a lower (0.85%—sample 6c), respectively higher (9.16%—sample 4c) mass loss in this region; this is most probably due to the preservation conditions, as the outer region samples all have a mass loss around 6%. The recorded mass losses are higher than those recorded for similar samples, originating from a site in the same region (*Sagu Site "A1_1",* previously presented by our group). The difference could be explained by a difference in environmental conditions of the analyzed sites. Also, no trend can be distinguished for this region, as some samples have a higher mass loss for samples *a* (1, 2, 4, 7), while the rest recorded a higher loss on samples *b*. The interior samples (samples *c*) are usually similar to the exteriors, with a lower weight loss recorded for samples 1c, 2c, 5c, and 6c, compared with the exterior samples. In the same time, the variation of the mass loss for samples *a/b* in this region could find explanation either in the use of these ceramics in ancient time [such as contact with water, as some authors suggest (Zvereva et al., 2019)] or to their orientation/contact with environmental factors during their burial in the soil, in either case being related to the humidity affecting the ceramics at some point (Drebushchak et al., 2005). Although the first explanation is acceptable, in our opinion, the last one is appliable in our case, thus explaining the inconsistencies between samples discovered in the same site. Thus, most probably, for the case with higher losses for the external parts (sides *b*) they were probably kept sealed for long period of times, with their original fillings.

The second stage appears in the region 200–approx. 560 °C. This is the stage where the decomposition of the hydroxyls occurs. The mass losses recorded for the samples are varying between 1.23% (sample 2c) and 6.40% (sample 1b) and can be associated with the presence of muscovite (as identified by XRD) in all samples.

The last major mass loss stage is recorded between approx. 550 °C and approx. 800 °C (as presented in **Table 4**). This stage contains the specific decomposition of calcite (700–800°C), and its presence is suggested in almost all samples (except 4 and 7), confirming both the XRD and XRF data (regarding the calcite/calcium content). The calcite suggested by XRD data in sample 7a is not confirmed by the TG curve, which can be explained either by its minor presence in the samples, a difference in the analyzed sample (due to the nature of the two methods), or by a combination of both factors (as the relatively low calcium content would suggest). The mass loss recorded in the region under 650 °C for some of the analyzed samples can be explained by the presence in higher amounts of kaolinite or illite (Lemma et al., 2018; Naimark et al., 2018). Other authors assign the decomposition in this stage to the combustion of organic material added into ceramic, or present as impurities in the samples (Moropoulou et al., 1995). More than that, the absence of the

endothermic event at 450 °C (except for samples 6a and 6b) associated with the dehydroxylation of kaolinite to the metastable metakaolin (Hajjaji et al., 2002; SperinckRaiteri et al., 2011) would suggest that the major clay mineral in the samples is represented by illite.

The final aspect record in the TG curves is represented by the mass gain recorded between the last temperature stage and 1,000 °C. The most probable explanation is represented by the transformation of the meta-clay to a spinel-type phase, as suggested by other authors (McConville and Lee, 2005; Shoval et al., 2011; Shoval and Paz, 2013).

The residues recorded at 1,000 °C vary greatly between samples. Thus, samples four and seven record residues over around 90%, respectively 93%, with relatively low differences between the two exterior sides. Samples 3, 5, and 6 also present a homogeneous behavior regarding the residues recorded on the analysis of the two exterior sides (86–88%). Sample 1 presents a relatively high difference between the two sides (88.2% for the inner side, respectively 85.3% for the outer side). This can be explained by the contribution of impurities (such as organic fragments, present only on the outer side). A special case is observed for sample 2: as visible from **Figure 1**, the sample presents white deposits on the exterior side (sample 2b). This led to different sampling, in order to analyze both the deposits and the ceramic material without any visible impurities. As such, high differences were obtained between the three analyzed samples (85.93% residue for the inner side/96.39% for 2b′, respectively 64.88% for 2b”); this is mainly due to the difference in terms of calcite content (very high on sample 2b”, as demonstrated by the higher weight loss recorded in the specific region). This could be explained by the presence of precipitated calcite, as other authors reported (Fabbri et al., 2014). The interior materials (samples c) usually have a higher residue (samples 1, 2, 3, and 5). The exceptions are sample 6 (with a relatively homogenous residue for all samples–86.73–87.55%), sample 4 (for which the *c* sample has a relatively low residue, compared with samples *a* and *b*) and sample 7 (for which the inner material has, however, a higher residue compared with their corresponding surfaces–7c’/7a, respectively 7c”/7b).

The most important conclusion from the thermal analyses is related to the interpretation of the overall analytic data. Samples four and six present a relatively homogenous thermal behavior on both inner and outer surfaces, confirming the similar composition on the two analyzed sides, as suggested by the other techniques. The main differences recorded between the different parts analyzed for these samples are related to the dehydration process (up to approx. 200 °C, samples *c* showing significant differences in this region). Sample 3, although presenting different surface characteristics, have a similar thermal behavior for all the analyzed areas, while samples one and two only present different surface composition (suggested by XRF and XRD) and different thermal behavior, supporting the variation in composition on the two sides. Relevant are also the residues recorded for samples one and two, with large differences recorded for the two analyzed sides. Sample 6, for which the TG curves suggest the presence of trace amounts of calcite, does not present neither a high calcium content (XRF), nor the specific peaks (XRD) for the *b* side. This is also the case of sample 7, for which the XRF/XRD data for sample 7a (presence of calcite) are not confirmed by TG data, which, furthermore, would suggests the presence of the particular mineral on sample 7b. Sample 5 (with a homogenous thermal behavior) also lacks the characteristics of calcite thermal degradation (as suggested by XRD/XRF data for sample 5a).

By corroborating all the analytical data, it seems that the analyzed samples can be classified in terms of calcite content as contaminant originating from the environment (even for the sample 2b), and not as containing the mineral in the original raw material. This conclusion is important for estimating the firing temperature, as its presence in the ceramic material would suggest lower temperatures. However, in our opinion, as the calcite originates from post-firing sources, the firing temperatures would be higher, around 800 °C (as the illite clay mineral would suffer a crystal reformation at temperatures in the range 850–920 °C (Araújo et al., 2004), in concordance with other LBA ceramics originating in Romania (Crandell et al., 2015), with the darker-colored ceramics exposed to even higher temperatures, most probably after manufacturing.

As a final remark, we underline the fact that the results of the analytical procedures applied should be interpreted as a sum of results, offering information mainly on the homogeneity of the samples and on the inhomogeneous presence of impurities.

CONCLUSION

If the major events and general developments of the most representative sites are already relatively well known, studies on LBA-specific material culture in this key region of the Carpathian Basin are insufficient. Recently, a series of analyzes on the stylistic evolution of ceramics in the Lower Mures was published. In order to achieve a more accurate characterization of the ceramics from the mentioned region, the stylistic analyzes (highlighting the main trends of ceramic shapes and decorations), must be doubled by archaeometry studies, which offer archaeologists new possibilities of interpretation on the artifacts. In this context, seven ceramic samples being dated to the Late Bronze Age (LBA) from two sites (Pecica–Site 14 and Sântana–Cetatea Veche—Old Fortress) were analyzed using a complex set of analytical techniques (thermal analysis, analysis based on ionizing radiation, Fourier-Transform Infrared spectroscopy and optical microscopy). The order of presenting the obtained results was chosen with two reasons: first of all, to propose an analytical methodology for this type of samples and secondly, complex results can only be presented if they are obtained by different techniques that provide information one to each other. Given the specific shape of the ceramic pieces and the burial conditions, all samples were analyzed on both sides, on the concave surface (interior of the vessels), respectively on the convex surface (exterior of the vessels).

As a general conclusion, by corroborating all the analytical data, it seems that the analyzed samples can be classified in terms of calcite content as contaminant originating from the environment, and not as containing the mineral in the original

raw material. This conclusion is important for estimating the firing temperature, as its presence in the ceramic material would suggest lower temperatures. However, in our opinion, as the calcite originates from post-firing sources, the firing temperatures would be higher, around 800 °C (as the illite clay mineral would suffer a crystal reformation at temperatures in the range 850–920 °C in concordance with other LBA ceramics originating in Romania, with the darker-colored ceramics exposed to even higher temperatures, most probably after manufacturing and sample 2 resembles the composition of the LBA ceramics of Anatolian origin. The two proposed indices (CIA/ICV), which are currently used by geologist to estimate the alteration/degradation of rocks or for the characterization of archaeological ceramic samples, indicate that two of the samples (2 and 3) could be categorized as exhibiting "little degradation effect" (CIA<50), while the rest present moderate degradation effect. These results indicate that the raw materials used for ceramic manufacturing undergone moderate weathering/alteration at source, without undergoing multiple weathering and lithification cycles (supporting the hypothesis that the raw materials consisted of sediments derived directly from an igneous source). Thus, most probably, for the case with higher losses for the external parts (sides b) they were probably kept sealed for long period of times, with their original fillings.

DATA AVAILABILITY STATEMENT

The raw data supporting the conclusions of this article will be made available by the authors, without undue reservation.

AUTHOR CONTRIBUTIONS

IF, and RF contributed to the conception and design of this study. II and VS provided the archaeological material, contributed to their placement in historical context and to the data interpretation. IF, AB, RB, TF and RF performed the XRF, XRD, and optical microscopy evaluation. VR performed FTIR analysis. CN performed TGA analysis. RF and IF wrote the first draft of the manuscript. VR and CN contributed to the discussion of the results and collaborated in the writing of the different sections of the manuscript. All authors contributed to the reading and review of the manuscript, and approved the submitted version.

FUNDING

The present work was partially supported by grants of the Romanian National Authority for Scientific Research and Innovation, CNCS/CCCDI–UEFISCDI, project number PN-III-P1-1.2-PCCDI-2017-0413, contract 50PCCDI/2018, within PNCDI III and project number PN-III-P2-2.1-PTE-2019-0579, contract 61PTE/2020, within PNCDI III.

SUPPLEMENTARY MATERIAL

The Supplementary Material for this article can be found online at: https://www.frontiersin.org/articles/10.3389/fmats.2021.630137/full#supplementary-material

REFERENCES

Abukhadra, M. R., and Mostafa, M. (2019). Effective Decontamination of Phosphate and Ammonium Utilizing Novel Muscovite/phillipsite Composite; Equilibrium Investigation and Realistic Application. *Sci. Total Environ.* 667, 101–111. doi:10.1016/j.scitotenv.2019.02.362

Araújo, J. H. D., Silva, N. F. D., Acchar, W., and Gomes, U. U. (2004). Thermal Decomposition of Illite. *Mat. Res.* 7, 359–361. doi:10.1590/s1516-14392004000200024

Bălan, G. (2013). "Fortified Settlements in the Area of Gáva Culture in Romania (In Romanian: Aşezările Fortificate Din Aria Culturii Gáva Din România)," in Lower Danube Prehistory. 50 years of excavation at Babadag (1962-2012) (in Romanian: Din Preistoria Dunarii de Jos. 50 de ani de la inceputul cercetarilor arheologice la Babadag (1962-2012))Proceedings of "Lower Danube Prehistory. 50 years of excavations at Babadag" Conference, Tulcea, Romania, 20-22 September. Editors SC Ailincăi, A Tarlea, and C Micu (Tulcea: . Istros: Brăila), 265–310.

Costa, T. G., de M. Correia, M. D., Reis, L. B., dos Santos, S. S., Machado, J. S., Bueno, L., et al. (2017). Spectroscopic Characterization of Recently Excavated Archaeological Potsherds of Taquara/Itararé Tradition from Tobias Wagner Site (Santa Catarina - Brazil). *J. Archaeological Sci. Rep.* 12, 561–568. doi:10.1016/j.jasrep.2017.03.014

Cox, R., Lowe, D. R., and Cullers, R. L. (1995). The Influence of Sediment Recycling and Basement Composition on Evolution of Mudrock Chemistry in the Southwestern United States. *Geochimica et Cosmochimica Acta* 59, 2919–2940. doi:10.1016/0016-7037(95)00185-9

Crandell, O., Ionescu, C., Giurgiu, A., Simon, V., Trandafir, D. L., and Nagy, J. (2015). "Pottery Firing Technology in the Late Bronze Age & Early Iron Age in NW Romania," in 6th Mineral Sciences in the Carpathians Conference, Veszprém, Hungary, 16–19 May, 2015. Editors G. B. Kiss (Szeged: Acta Mineralogica-Petrographica Abstract Series), 9, 5.

Crocombe, R. A. (2018). Portable Spectroscopy. *Appl. Spectrosc.* 72, 1701–1751. doi:10.1177/0003702818809719

De Benedetto, G. E., Laviano, R., Sabbatini, L., and Zambonin, P. G. (2002). Infrared Spectroscopy in the Mineralogical Characterization of Ancient Pottery. *J. Cult. Heritage* 3, 177–186. doi:10.1016/s1296-2074(02)01178-0

Diskin, S., and Ashley, C. (2016). Characterisation of Archaeological Ceramics from the Khwebe Hills of Northern Botswana. *J. Archaeological Sci. Rep.* 6, 574–583. doi:10.1016/j.jasrep.2016.03.033

Drebushchak, V. A., Mylnikova, L. N., Drebushchak, T. N., and Boldyrev, V. V. (2005). The Investigation of Ancient Pottery. *J. Therm. Anal. Calorim.* 82, 617–626. doi:10.1007/s10973-005-0942-9

Drebushchak, V. A., Mylnikova, L. N., and Drebushchak, T. N. (2018). Thermoanalytical Investigations of Ancient Ceramics. *J. Therm. Anal. Calorim.* 133, 135–176. doi:10.1007/s10973-018-7244-5

Duran, A., Perez-Maqueda, L. A., Poyato, J., and Perez-Rodriguez, J. L. (2010). A thermal Study Approach to Roman Age wall Painting Mortars. *J. Therm. Anal. Calorim.* 99, 803–809. doi:10.1007/s10973-009-0667-2

El Amraoui, M., Haddad, M., Bejjit, L., Ait Lyazidi, S., and Lakhal, R. (2017). On-site XRF Characterization of Archaeological Materials in CERA center of Rissani (Morocco). *IOP Conf. Ser. Mater. Sci. Eng.* 186, 012029. doi:10.1088/1757-899x/186/1/012029

El-Gohary, M., El-Ghareb, W., and Saad, M. (2019). Damage Quantification of Archaeological Pottery in Sheikh Hamad "Athribis" Sohag-Egypt. *Ceramics Int.* 45, 17611–17619. doi:10.1016/j.ceramint.2019.05.326

Fabbri, B., Gualtieri, S., and Shoval, S. (2014). The Presence of Calcite in Archeological Ceramics. *J. Eur. Ceram. Soc.* 34, 1899–1911. doi:10.1016/j.jeurceramsoc.2014.01.007

Fierascu, R. C., Fierascu, I., Baroi, A. M., Brazdis, R. I., Fistos, T., Nicolae, C. A., et al. (2020). Characterization of Historical Ceramics: a Case Study. *Rom. Rep. Phys.* 72, 801.

Fierascu, R. C., Fierascu, I., Ortan, A., Constantin, F., Mirea, D. A., and Statescu, M. (2017). Complex Archaeometallurgical Investigation of Silver Coins from the XVI Th -XVIII Th century. *Nucl. Instr. Methods Phys. Res. Section B: Beam Interactions Mater. Atoms* 401, 18–24. doi:10.1016/j.nimb.2017.04.030

Gogaltan, F., Sava, V., and Krause, R. (2019). "First Steps in the Dating of the Bronze Age Mega-Fort in Sântana-CetateaVeche (Southwestern Romania)" in Bronze Age Fortresses in Europe.Proceedings of the Second International LOEWE Conference, 9-13 October 2017. Editors S Hansen and R Krause (Bonn: Universitätsforschungen zur prähistorischen Archäologie 335LOEWE-Schwerpunkt Prähistorische Konfliktforschung), 161–176.

Gogaltan, F., Sava, V., Krause, R., and Veche, S-C. (2019). "A Late Bronze Age Mega-Fort in the Lower Mureș Basin in Southwestern Romania," in Materialisation of Conflicts. Proceedings of the Third International LOEWE Conference, Fulda, 24th - 27th September 2018. Editors S Hansen and R Krause (Bonn: . Habelt Verlag), 191–221.

Gogaltan, F., Sava, V., and Sântana, C. V. (2010). *A Bronze Age earthwork on the lower Mureș (In Romanian: Sântana Cetatea Veche. O fortificație de pământ a epocii bronzului la Mureșul de jos)*. Arad: Complexul Muzeal Arad.

Gogaltan, F. (2015). "The Early and Middle Bronze Age Chronology on the Eastern Frontier of the Carpathian Basin: Revisited after 15 Years," in Bronze Age Chronology in the Carpathian Basin: Proceedings of the International Colloquium from Târgu Mureș, 2-4 October 2014. Editors RE Németh and R Botond (Mega: Cluj-Napoca), 53–95.

Gutsuz, P., Kibaroğlu, M., Sunal, G., and Hacıosmanoğlu, S. (2017). Geochemical Characterization of clay Deposits in the Amuq Valley (Southern Turkey) and the Implications for Archaeometric Study of Ancient Ceramics. *Appl. Clay Sci.* 141, 316–333. doi:10.1016/j.clay.2017.03.004

Hajjaji, M., Kacim, S., and Boulmane, M. (2002). Mineralogy and Firing Characteristics of a Clay from the Valley of Ourika (Morocco). *Appl. Clay Sci.* 21, 203–212. doi:10.1016/s0169-1317(01)00101-6

Hein, A., and Kilikoglou, V. (2018). Modeling of the Microstructure of Ancient Functional Ceramics and Assessment of Their Performance. *Proced. Struct. Integrity* 10, 219–226. doi:10.1016/j.prostr.2018.09.031

Hoeck, V., Ionescu, C., Ghergari, L., and Precup, C. (2009). Towards Mineralogical and Geochemical Reference Groups for Some Bronze Age Ceramics from Transylvania (Romania). *Studia. UBB. Geologia* 54, 41–51. doi:10.5038/1937-8602.54.2.8

Holakooei, P., Tessari, U., Verde, M., and Vaccaro, C. (2014). A New Look at XRD Patterns of Archaeological Ceramic Bodies. *J. Therm. Anal. Calorim.* 118, 165–176. doi:10.1007/s10973-014-4012-z

Ignat, A., and Sava, V. (2019). Late Bronze Age Funerary Practices in the Lower Mureș Basin. *Revista Arheologică.* 15, 5–20.

Ionescu, C., Hoeck, V., Gruian, C., and Simon, V. (2014). Insights into the EPR Characteristics of Heated Carbonate-Rich Illitic clay. *Appl. Clay Sci.* 97-98, 138–145. doi:10.1016/j.clay.2014.05.023

Jordá, J. D., Jordán, M. M., Ibanco-Cañete, R., Montero, M. A., Reyes-Labarta, J. A., Sánchez, A., et al. (2015). Mineralogical Analysis of Ceramic Tiles by FTIR: A Quantitative Attempt. *Appl. Clay Sci.* 115, 1–8. doi:10.1016/j.clay.2015.07.005

Kloužková, A., Kavanová, M., Kohoutková, M., Zemenová, P., and Dragoun, Z. (2016). Identification of Causes of Degradation of Gothic Ceramic Tiles by thermal Analyses. *J. Therm. Anal Calorim* 125, 1311–1318. doi:10.1007/s10973-016-5488-5

Krause, R., Szentmiklosi, A., Heeb, B., Lehmphul, R., Teinz, K., Bălărie, A., et al. (2016). Cornești-Iarcuri: Die Ausgrabungen 2013 und 2014 in der befestigten Großsiedlung der späten Bronzezeit im Rumänischen Banat. *Eurasia Antiq* 22, 133–184.

Legodi, M., and Dewaal, D. (2007). The Preparation of Magnetite, Goethite, Hematite and Maghemite of Pigment Quality from Mill Scale Iron Waste. *Dyes Pigm.* 74, 161–168. doi:10.1016/j.dyepig.2006.01.038

Lehmphul, R., Heeb, B., Szentmiklosi, A., Stobbe, A., and Krause, R. (2019). "The Genesis of the Fortification of Cornești-Larcuri Near the Mureș Lower Course (Romanian Banat) – A Phase Model on the Chronology of the Settlement and Fortification Structures," in Bronze Age Fortresses in Europe. Proceedings of the Second International LOEWE Conference, Alba Iulia (Romania), 9-13 October 2017. Editors S Hansen and R Krause (Bonn: . Universitätsforschungen zur prähistorischen Archäologie 335LOEWE-Schwerpunkt Prähistorische Konfliktforschung), 253–278.

Lemma, R., Castellano, C. C., Bonavetti, V. L., Trezza, M. A., Rahhal, V. F., and Irassar, E. F. (2018). "Thermal Transformation of Illitic-Chlorite Clay and its Pozzolanic Activity," in *Calcined Clays for Sustainable Concrete. RILEM Bookseries*. Editors F Martirena, A Favier, and K Scrivener (Dordrecht: Springer), 266–272.

McConville, C. J., and Lee, W. E. (2005). Microstructural Development on Firing Illite and Smectite Clays Compared with that in Kaolinite. *J. Am. Ceram. Soc.* 88, 2267–2276. doi:10.1111/j.1551-2916.2005.00390.x

Molloy, B., Jovanović, D., Bruyère, C., Marić, M., Bulatović, J., Mertl, P., et al. (2020). A New Bronze Age Mega-Fort in Southeastern Europe: Recent Archaeological Investigations at Gradište Iđoš and Their Regional Significance. *J. Field Archaeology* 45, 293–314. doi:10.1080/00934690.2020.1734899

Moropoulou, A., Bakolas, A., and Bisbikou, K. (1995). Thermal Analysis as a Method of Characterizing Ancient Ceramic Technologies. *Thermochim. Acta* 269-270, 743–753. doi:10.1016/0040-6031(95)02570-7

Naimark, E. B., Boeva, N. M., Kalinina, M. A., and Zaytseva, L. V. (2018). Complementary Transformations of Buried Organic Residues and the Ambient Sediment: Results of Long-Term Taphonomic Experiments. *Paleontol. J.* 52, 109–122. doi:10.1134/s0031030118020053

Nesbitt, H. W., and Young, G. M. (1982). Early Proterozoic Climates and Plate Motions Inferred from Major Element Chemistry of Lutites. *Nature* 299, 715–717. doi:10.1038/299715a0

Palanivel, R., and Rajesh Kumar, U. (2011). Thermal and Spectroscopic Analysis of Ancient Potteries. *Rom. Rep. Phys.* 56, 195–208.

Papadopoulou, D. N., Lalia-Kantouri, M., Kantiranis, N., and Stratis, J. A. (2006). Thermal and Mineralogical Contribution to the Ancient Ceramics and Natural Clays Characterization. *J. Therm. Anal. Calorim.* 84, 39–45. doi:10.1007/s10973-005-7173-y

Papadopoulou, D., Zachariadis, G., Anthemidis, A., Tsirliganis, N., and Stratis, J. (2006). Development and Optimisation of a Portable Micro-XRF Method for *In Situ* Multi-Element Analysis of Ancient Ceramics. *Talanta* 68, 1692–1699. doi:10.1016/j.talanta.2005.08.051

Papakosta, V., Lopez-Costas, O., and Isaksson, S. (2020). Multi-method (FTIR, XRD, PXRF) Analysis of Ertebølle Pottery Ceramics from Scania, Southern Sweden. *Archaeometry* 62, 677–693. doi:10.1111/arcm.12554

Paterakis, A. B., and Steiger, M. (2015). Salt Efflorescence on Pottery in the Athenian Agora: A Closer Look. *Stud. Conserv* 60, 172–184. doi:10.1179/2047058413Y.0000000113

Ponta, O., Vulpoi, A., Zirra, V. V., and Simon, S. (2016). Structural and Compositional Investigation of Ancient Ceramics from a Fortified Settlement in South-Western Romania. *J. Mol. Struct.* 1122, 157–163. doi:10.1016/j.molstruc.2016.05.100

Ramasamy, V., Rajkumar, P., and Ponnusamy, V. (2009). Depth wise Analysis of Recently Excavated Vellar River Sediments through FTIR and XRD Studies. *Indian J. Phys.* 83, 1295–1308. doi:10.1007/s12648-009-0110-3

Ricci, G., Caneve, L., Pedron, D., Holesch, N., and Zendri, E. (2016). A Multi-Spectroscopic Study for the Characterization and Definition of Production Techniques of German Ceramic Sherds. *Microchemical J.* 126, 104–112. doi:10.1016/j.microc.2015.12.009

Rizzo, G., Sansone, M. T. C., Perri, F., and Laurita, S. (2016). Mineralogy and Petrology of the Metasedimentary Rocks from the Frido Unit (Southern Apennines, Italy). *Period Mineral.* 85, 153–168. doi:10.2451/2016PM630

Russell, J. D., and Fraser, A. R. (1994). "Infrared Methods," in *Clay Mineralogy: Spectroscopic and Chemical Determinative Methods*. Editor MJ Wilson (Dordrecht: Springer), 11–67. doi:10.1007/978-94-011-0727-3_2

Sava, V., and Gogaltan, F. (2019). "Lower Mures basin at the beginning of the Late Bronze Age (1600/1500-1400 BC) (In Romanian: Bazinul Mureșului de Jos la începutul bronzului târziu (1600/1500-1400 BC))," in *In Honorem Prof. Univ. Dr. Sabin Adrian Luca: History and Destiny (In Romanian: In Honorem Prof. Univ. Dr. Sabin Adrian Luca: Istorie Și destin)*. Editor DR Hrib (Sibiu: Brukenthal National Museum Publishing House), 223–234.

Sava, V., Hurezan, G. P., and Mărginean, F. (2012). Late Bronze Age Metal Artefacts Discovered in Șagu, Site "A1_1", Arad – Timișoara Highway (Km 0+19.900-0+20.620). *Ziridava Studia Archaeologica* 26, 83–107.

Sava, V., Hurezan, G. P., and Mărginean, F. (2011). *Şagu "Sit A1_1" a Late Bronze Age Settlement on the Lower Mureş*. Cluj-Napoca, Romania: Mega.

Sava, V. (2020). The Late Bronze Age Pottery in the South-Eastern Carpathian Basin. *slovarch* 68, 253–296. doi:10.31577/slovarch.2020.68.12

Sava, V. (2019). The Late Bronze Age Settlement at şagu and the Early Use of the Channeled Pottery. *Analele Banatului* 27, 109–145.

Semiz, B., Abay, E., Dedeoğlu, F., Konakçi, E., and Ozan, A. (2018). An Archaeometric Investigation of Early and Middle Bronze Age Pottery from the Upper Meander Basin in Southwestern Anatolia. *Mediterr. Archaeol Archaeom* 18, 121–150.

Shoval, S., Boudeulle, M., and Panczer, G. (2011). Identification of the thermal Phases in Firing of Kaolinite to Mullite by Using Micro-raman Spectroscopy and Curve-Fitting. *Opt. Mater.* 34, 404–409. doi:10.1016/j.optmat.2011.08.031

Shoval, S., and Paz, Y. (2013). A Study of the Mass-Gain of Ancient Pottery in Relation to Archeological Ages Using thermal Analysis. *Appl. Clay Sci.* 82, 113–120. doi:10.1016/j.clay.2013.06.027

SperinckRaiteri, S. P., Raiteri, P., Marks, N., and Wright, K. (2011). Dehydroxylation of Kaolinite to Metakaolin-A Molecular Dynamics Study. *J. Mater. Chem.* 21, 2118–2125. doi:10.1039/c0jm01748e

Sun, H., Liu, M., Li, L., Yan, L., Zhou, Y., and Feng, X. (2020). A New Classification Method of Ancient Chinese Ceramics Based on Machine Learning and Component Analysis. *Ceramics Int.* 46, 8104–8110. doi:10.1016/j.ceramint.2019.12.037

Wang, W., Cong, J., Deng, J., Weng, X., Lin, Y., Huang, Y., et al. (2018). Developing Effective Separation of Feldspar and Quartz while Recycling Tailwater by HF Pretreatment. *Minerals* 8, 149. doi:10.3390/min8040149

Zvereva, I. A., Kuznetsov, V. M., Zhukov, Y. M., Mazurkevich, A. N., and Dolbunova, E. V. (2019). Thermal Analysis and Multi-Analytical Comparison of Samples of Neolithic Ceramics from Dnepr-Dvina and Low Don Regions. *J. Therm. Anal. Calorim.* 138, 1879–1886. doi:10.1007/s10973-019-08621-x

Conflict of Interest: The authors declare that the research was conducted in the absence of any commercial or financial relationships that could be construed as a potential conflict of interest.